ELSEVIER

Water Research 38 (2004) 1305–1317

WATER RESEARCH

www.elsevier.com/locate/watres

Modelling particle size distribution dynamics in marine waters

Xiao-yan Li*, Jian-jun Zhang, Joseph H.W. Lee

Department of Civil Engineering, Environmental Engineering Research Centre, The University of Hong Kong, Pokfulam Road, Hong Kong, China

Received 4 June 2003; received in revised form 31 October 2003; accepted 7 November 2003

Abstract

Numerical simulations were carried out to determine the particle size distribution (PSD) in marine waters by accounting for particle influx, coagulation, sedimentation and breakage. Instead of the conventional rectilinear model and Euclidean geometry, a curvilinear collision model and fractal scaling mathematics were used in the models. A steady-state PSD can be achieved after a period of simulation regardless of the initial conditions. The cumulative PSD in the steady state follows a power-law function, which has three linear regions after log–log transformation, with different slopes corresponding to the three collision mechanisms, Brownian motion, fluid shear and differential sedimentation. The PSD slope varies from −3.5 to −1.2 as a function of the size range and the fractal dimension of the particles concerned. The environmental conditions do not significantly alter the PSD slope, although they may change the position of the PSD and related particle concentrations. The simulation demonstrates a generality in the shape of the steady-state PSD in the ocean, which is in agreement with many field observations. Breakage does not affect the size distribution of small particles, while a strong shear may cause a notable change in the PSD for larger and fractal particles only. The simplified approach of previous works using dimensional analysis still offers valuable approximations for the PSD slopes, although the previous solutions do not always agree with the simulation results. The variation in the PSD slope observed in field investigations can be reproduced numerically. It is argued that non-steady-state conditions in natural waters could be the main reason for the deviation of PSD slopes. A change in the nature of the particles, such as stickiness, and environmental variables, such as particle input and shear intensity, could force the PSD to shift from one steady state to another. During such a transition, the PSD slope may vary to some extent with the particle population dynamics.

Keywords: Coagulation; Flocculation; Fractal; Marine water; Particle; Particle size distribution (PSD); Phytoplankton bloom

1. Introduction

Particulate materials in the ocean play an important role in the transport of many substances, including biogenic matter, trace metals and organic pollutants, from surface waters to, eventually, the ocean floor. Natural particles can vary widely in size from sub-micron colloids to larger aggregates of a few millimetres, such as marine snow. Field observations indicate that the particle population in marine waters has a size distribution that may be fitted by a power-law function, i.e., $N(l) \sim l^{-b}$, where $N(l)$ is the cumulative number concentration of particles of size l or larger, and $-b$ is defined as the slope of the size distribution [1–7]. Despite vast differences in particle properties and environmental conditions in different waters, the size distribution slopes are found to vary within a narrow range only, which is mainly from −1.5 to −4.0, particularly for particles smaller than 100 μm (Table 1). Field observations suggest a generality in the shape of the size distribution of marine particles, which, however, remains to be established theoretically.

Particle coagulation has been considered to play a major role in determining the particle size distribution

*Corresponding author. Tel.: +852-2859-2659; fax: +852-2559-5337.

E-mail address: xlia@hkucc.hku.hk (X.-Y. Li).

0043-1354/$ - see front matter © 2003 Elsevier Ltd. All rights reserved.
doi:10.1016/j.watres.2003.11.010

Table 1
Slopes of the cumulative particle size distributions ($\log N(l)$ vs. l) predicted by dimensional analysis and observed in the ocean and a mesecosm

Dominant collision mechanism assumed Approximate size range	Brownian motion $<2\,\mu m$	Fluid shear $2\sim60\,\mu m$	Differential sedimentation $>60\,\mu m$	References
Dimensional analysis:				
Hunt	−1.5	−3.0	−3.5	[1]
Jiang and Logan: (D: fractal dimension)	$-\frac{D}{2}$	$-\frac{1}{2}(D+3)$	$-\frac{1}{2}(1+2D)$ (Stokes' settling, $D\geqslant2$)	[13]
Observations:				
(a) Natural waters:				
N. Atlantic Ocean		-2.7 ± 0.2	−3.6	[41]
		-3.0 ± 0.3	−4.1	[42]
Gulf of Mexico	−1.6	−3.4	−4.0	[43]
S. Atlantic Ocean			$-2.8\sim-7.7$	[44]
E. Pacific Ocean		−3.3		[45]
			$-1.8\sim-11.0$	[46]
California coastal		-2.8 ± 0.2		[1]
Ocean (unidentified)	−1.5	−1.5		[3]
E. Pacific coastal				[5]
Monterey Bay-1		-1.8 ± 0.2	-1.8 ± 0.2	
Monterey Bay-2		-1.5 ± 0.1	-1.5 ± 0.1	
East Sound		-2.0 ± 0.2	-2.0 ± 0.2	
(b) Phytoplankton bloom in a mesocosm		$-1.2\sim-1.8$	$-1.2\sim-1.8$	[30]

(PSD) in natural waters [1,5,8–13]. The dynamics of particle interactions and the resulting size distribution can be modelled using the approach of Smoluchowski's equation [14–17]. However, the Smoluchowski formulation is too complicated to be solved analytically. Hunt [1,11] used dimensional analysis to simplify the coagulation equation and attained an approximation of the steady-state PSD slope. As oceanic particles have been found to be fractal in nature [2,18,19], Jiang and Logan [13] extended Hunt's work to fractal particles and included the fractal scaling relationship in the calculation. The result gave three linear regions in the particle size distribution in accordance with the three collision mechanisms, Brownian motion, fluid shear and differential sedimentation, operating in different size ranges. The value of the PSD slope is only a function of the size range and the fractal dimension of the particles, and is independent of other environmental and process factors (Table 1). The analytical approximations from dimensional analysis show the general shape of the PSD in the ocean.

However, the application of dimensional analysis to the PSD problem relies on a number of important assumptions, many of which do not necessarily hold in actual situations [14]. The most critical, but also questionable, assumptions include: (1) that collisions occur only between particles of similar sizes for which only one collision mechanism dominates, and (2) all particle mass moves through the size distribution to the largest particles, which are removed from the system by settling. Moreover, the analytical solutions are derived based on the rectilinear collision model, which has been known to over-predict particle collision kinetics to a great extent [17,20–22]. These unrealistic assumptions and the rectilinear model used by dimensional analysis largely undermine its results for PSD slopes. Apart from the general shape, dimensional analysis provides little information about particle population dynamics in marine waters.

A numerical technique can be used to solve the Smoluchowski equation without using the above assumptions [12,17,23–25]. Burd and Jackson [14] applied the sectional method to simulate particle dynamics in the ocean. The simulation reached a steady-state size distribution in a particle system while accounting for a consistent particle influx, coagulation, sedimentation and breakage processes. They found that the numerically simulated PSD slopes do not always agree with those predicted by dimensional analysis. The assumptions underlying dimensional analysis are mainly responsible for the disagreement. Nonetheless, their mathematical simulation was still based on the unrealistic rectilinear model. The impact of the fractal scaling property of marine particles on the size distribution was not fully investigated, and the simulated distributions were not used to reconcile the findings of field surveys for the PSD slope or its variation.

In the present study, an improved numerical approach was used to simulate the particle size distribution in marine waters. The methodological improvements included a modified sectional method [17], the application of fractal scaling mathematics, and a new curvilinear

collision model developed by Han and Lawler [20]. The simulation results were compared with the previous dimensional analysis and field observations of the shape of particle size distributions. The generality of marine PSD was verified in terms of the slope values. In addition, a simulation of the transition between the status of different steady states and related particle population dynamics helped to explain the variation in the slope values observed in the field.

2. Theory and methods

2.1. Flocculation equation

The flocculation process in a system of heterodisperse particles has been modelled by the change in particle size distribution [14,23,24,26–28]. When simultaneous actions of particle influx, coagulation, sedimentation and breakage are considered, the particle size distribution dynamics can be described in the form of the Smoluchowski equation given below:

$$\frac{dn(m)}{dt} = \frac{1}{2}\int_0^m \alpha\beta(m-m',m')n(m-m')n(m')\,dm' - n(m)\int_0^\infty \alpha\beta(m,m')n(m')\,dm' - s(m)n(m) + \int_m^\infty \gamma(m,m'')s(m'')n(m'')\,dm'' - \frac{u(m)}{H}n(m) + \phi(m), \quad (1)$$

where t is time, $n(m)$ is the particle size density function with respect to the particle size measured by mass, m, m' is the mass of another particle, which is smaller than m in the first term on the right-hand side of the equation, β is the collision frequency function describing the rate of contacts between the particles indicated, α is the collision efficiency defined as fraction of collisions that result in particle attachment, $s(m)$ is the break-up rate function, $\gamma(m,m'')$ is the breakage distribution function defining the mass fraction of fragments of size m breaking from a larger aggregate of size m'', H is the depth of the water column, $u(m)$ is the settling velocity and $\phi(m)$ is the input rate of the particles concerned.

The sectional approximation has been employed to find numerical solutions to Eq. (1). Following the common approach of the sectional method [12,16,17,23], the size sections are so generated that the upper bound of a section is twice its lower bound in terms of mass, e.g., $m_k = 2m_{k-1}$ for section k. Within each size section, it is assumed here that the particle mass is distributed uniformly along the log-scale, which gives a particle size density function of $n(m) = Q_k/((\ln 2)m^2)$, where Q_k is the particle mass concentration in the kth section [17]. Subsequently, Eq. (1) can be converted to

$$\frac{dQ_k}{dt} = Q_{k-1}\sum_{i=1}^{k-1} {}^1B_{i,k-1,k}Q_i + Q_k\sum_{i=1}^{k} {}^2B_{i,k,k}Q_i - Q_k\sum_{i=1}^{k} {}^3B_{i,k,k}Q_i - {}^4B_{k,k,k}Q_k^2 - Q_k\sum_{i=k+1}^{s} {}^5B_{k,i,k}Q_i - {}^1S_kQ_k + \sum_{i=k+1}^{s} {}^2S_{k,i}Q_i - U_kQ_k + q_k, \quad (2)$$

where i signifies the section number and s is the last size section. Eq. (2) is the governing equation for modelling particle size dynamics in an open system, such as marine waters. For any given section, such as section k, there is a total of nine cases of particle input, attachment, breakage and sedimentation involved in the mass movement. Table 2 illustrates the nine particle transport and transformation processes that result in the gain and loss of particle mass in the kth section. ${}^1B_{i,k-1,k}$, ${}^2B_{i,k,k}$, ${}^3B_{i,k,k}$, ${}^4B_{k,k,k}$ and ${}^5B_{k,i,k}$ are the sectional coagulation coefficients, ${}^1S_k$ and ${}^2S_{k,i}$ are the sectional breakage coefficients, U_k is the sectional settling velocity and q_k is the sectional particle input rate. The computation of these sectional coefficients is also summarized in Table 2. Eq. (2) represents a finite number of coupled ordinary differential equations for the change in particle concentrations in all the size sections. These differential equations can readily be solved using the fourth-order Runge–Kutta method with a constant time step of 1 s, as described elsewhere [17,28].

2.2. Fractal aggregates

Although mass is used to track particle transport between size sections, the rates of particle coagulation and breakup depend more directly on the actual length of the particles. Natural particles have been characterized as fractals with a highly porous and amorphous structure [2,5,13,18,29]. For fractal particles, the length, l, can be related to the mass by $m \sim l^D$, or

$$l = c\left(\frac{m}{\rho_p}\right)^{1/D}, \quad (3)$$

where ρ_p is the density of primary particles and c is an empirical constant [13,30]. The settling velocity of a fractal particle can be calculated using Stokes' law, or

$$u(m) = \frac{g(\rho_p - \rho_l)m}{3\pi\mu\rho_p l}, \quad (4)$$

where g is the gravitational constant, ρ_l is the density and μ is the viscosity of the liquid [31,32].

Table 2
Different particle transport cases and related sectional rate coefficients

Case	Symbol	Description	Illustration	Calculation $f(m_x, m_y) = (\alpha\beta(m_x, m_y))/((\ln 2)^2 m_x^2 m_y^2)$
1 Gain	${}^1B_{i,j,k}$	Newly formed doublet moving into the kth section ($m_{k-1} < (m_x + m_y) < m_k$); $m_0 \leqslant m_x \leqslant m_{k-1}$ and $m_{k-2} \leqslant m_y < m_{k-1}$; $i \leqslant k-1$, $j = k-1$.	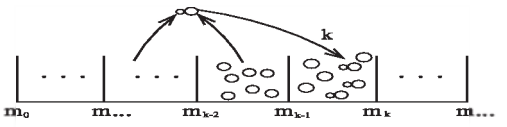	$\int_{m_{i-1}}^{m_i} \int_{m_{k-1}-m_x}^{m_{k-1}} (m_x + m_y) f(m_x, m_y)\, \mathrm{d}m_x\, \mathrm{d}m_y$
2 Gain	${}^2B_{i,j,k}$	Newly formed doublet in the kth section ($m_{k-1} < (m_x + m_y) < m_k$); $m_0 \leqslant m_x < m_{k-1}$ and $m_{k-1} \leqslant m_y < m_k$; $i < k, j = k$.	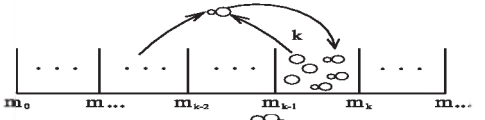	$\frac{1}{2}\int_{m_{k-2}}^{m_{k-1}} \int_{m_{k-2}}^{m_{k-1}} (m_x + m_y) f(m_x, m_y)\, \mathrm{d}m_x\, \mathrm{d}m_y$ $\int_{m_{i-1}}^{m_i} \int_{m_{k-1}}^{m_k - m_x} m_x f(m_x, m_y)\, \mathrm{d}m_x\, \mathrm{d}m_y$
3 Loss	${}^3B_{i,j,k}$	A particle being moved out of the kth section by attachment to a smaller particle ($m_k < (m_x + m_y)$); $m_0 \leqslant m_x < m_{k-1}$ and $m_{k-1} \leqslant m_y < m_k$; $i < k, j = k$.	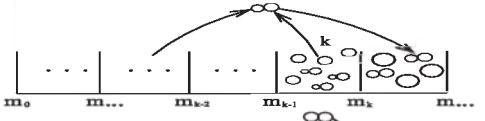	$\int_{m_{i-1}}^{m_i} \int_{m_{k-1}}^{m_k - m_x} m_y f(m_x, m_y)\, \mathrm{d}m_x\, \mathrm{d}m_y$
4 Loss	${}^4B_{i,j,k}$	A particle being moved out of the kth section by attachment to a similarly sized particle; ($m_k < (m_x + m_y)$); $m_{i-1} \leqslant m_x < m_i$ and $m_{i-1} \leqslant m_y < m_k$; $i = k, j = k$.	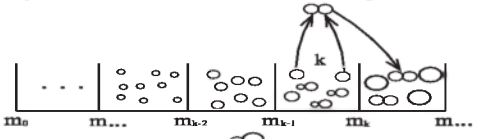	$\frac{1}{2}\int_{m_{k-1}}^{m_k} \int_{m_{k-1}}^{m_k} (m_x + m_y) f(m_x, m_y)\, \mathrm{d}m_x\, \mathrm{d}m_y$
5 Loss	${}^5B_{k,i,j}$	A particle being moved out of the kth section by attachment to a larger particle ($m_k < (m_x + m_y)$); $m_{i-1} \leqslant m_x < m_i$ and $m_i \leqslant m_y$; $i = k, j > k$	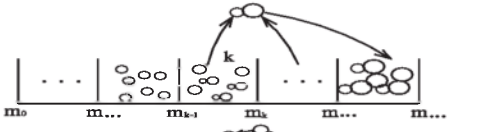	$\int_{m_{k-1}}^{m_k} \int_{m_{j-1}}^{m_j} m_y f(m_x, m_y)\, \mathrm{d}m_x\, \mathrm{d}m_y$
6 Loss	${}^1S_k$	Particles being moved out of the kth section by breakage, $m_{k-1} < m < m_k$.	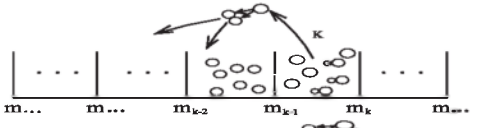	$\int_{m_{k-1}}^{m_k} \frac{s(m)}{m \ln 2}\, \mathrm{d}m$
7 Gain	${}^2S_{k,i}$	Particle fragments moving into the kth section by breakage of larger particles, $m_{k-1} < m < m_k$ and $m_{i-1} < m_z < m_i$; $k < i$.	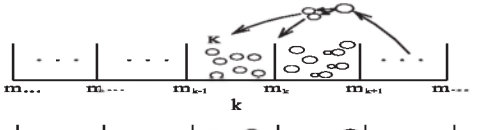	$\int_{m_{k-1}}^{m_k} \int_{m_{i-1}}^{m_i} \frac{\gamma(m, m_z) s(m_z)}{m_z \ln 2}\, \mathrm{d}m_z\, \mathrm{d}m$
8 Loss	U_k	Particles moving out of the kth section by sedimentation, $m_{k-1} < m < m_k$.		$\int_{m_{k-1}}^{m_k} \frac{u(m)}{H \cdot m \ln 2}\, \mathrm{d}m$
9 Gain	Q_k	Particles inputting into the kth section, $m_{k-1} < m < m_k$.	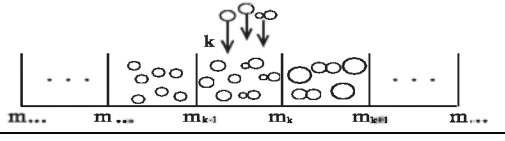	$\int_{m_{k-1}}^{m_k} \phi(m) m\, \mathrm{d}m$

2.3. Coagulation models

The rectilinear collision model, which assumes that particles move in straight lines until a collision occurs, has the following formulations for the collision frequency functions of the three collision mechanisms.

Brownian motion:

$$\beta_{\mathrm{Br}}(i,j) = \frac{2kT}{3\mu}\left(\frac{1}{l_i} + \frac{1}{l_j}\right)(l_i + l_j). \tag{5a}$$

Fluid shear:

$$\beta_{\mathrm{Sh}}(i,j) = \frac{G}{6}(l_i + l_j)^3. \tag{5b}$$

Differential sedimentation:

$$\beta_{\mathrm{DS}}(i,j) = \frac{\pi}{4}(l_i + l_j)^2\left|u_i - u_j\right|, \tag{5c}$$

where k is Boltzmann's constant, T is the absolute temperature, and G is the shear rate which is a measurement of the turbulence intensity in water. The total interparticle collision frequency function is the sum of these three independent mechanisms, i.e.,

$$\beta(i,j) = \beta_{\mathrm{Br}}(i,j) + \beta_{\mathrm{Sh}}(i,j) + \beta_{\mathrm{DS}}(i,j). \tag{6}$$

The curvilinear collision model takes into account hydrodynamic interactions and short-range forces between approaching particles, which results in reduced, but more realistic, collision frequencies between impermeable particles [20,21,33,34]. According to Han and Lawler [20], the curvilinear β_{cur} can be related to the well-defined rectilinear β by the reduction factors, i.e.,

$$\beta_{\mathrm{cur}}(i,j) = e_{\mathrm{Br}}\beta_{\mathrm{Br}}(i,j) + e_{\mathrm{Sh}}\beta_{\mathrm{Sh}}(i,j) + e_{\mathrm{DS}}\beta_{\mathrm{DS}}(i,j), \tag{7}$$

where e_{Br}, e_{Sh} and e_{DS} are the curvilinear reduction factors for the collision mechanisms indicated. Based on their numerical solutions, Han and Lawler [20] suggested the following estimations for these factors:

$$e_{\mathrm{Br}} = a + b\lambda + c\lambda^2 + d\lambda^3, \tag{8a}$$

$$e_{\mathrm{Sh}} = \frac{8}{(1+\lambda)^3}10^{(a+b\lambda+c\lambda^2+\mathrm{d}\lambda^3)}, \tag{8b}$$

$$e_{\mathrm{DS}} = 10^{(a+b\lambda+c\lambda^2+\mathrm{d}\lambda^3)}, \tag{8c}$$

where λ is the size ratio ($0<\lambda\leqslant 1$) between the two colliding particles, and $a-d$ are the intermediate coefficients. Although the same letters are used, these coefficients are completely different in each of the equations given above. The values of $a-d$ were given by Han and Lawler [20] in discrete form in three tables for the three collision mechanisms. To make their results more available for use in mathematical simulations, non-linear regressions were conducted in an earlier work to transform the discrete data into 14 fitting formulations [17]. The regression equations are used here to compute the curvilinear reduction factors in Eqs. (8a)–(8c), and hence obtain the curvilinear collision frequency functions.

2.4. Breakage rate and breakage distribution functions

Particle breakage is brought about mainly by fluid shear stress, and the fragility of a particle aggregate is generally proportional to its size [27,35–37]. The breakage rate coefficient has been written as a function of the shear intensity, G, and the particle size in volume, V [27,38,39], or $s(V) = EG^bV^{1/3}$, where E and b are the breakage rate constants. This equation can also be converted to become a function of the shear rate and particle mass, as given below:

$$s(m) = E'G^bm^{1/D}, \tag{9}$$

where $E' = (\pi/6)^{1/3}(1/\rho_{\mathrm{p}})^{1/D}cE$. The pair $E = 7.0\times10^{-4}$ and $b = 1.6$, which have been used in previous studies [26,28], are adopted in the present numerical simulation.

For the breakage of a particle aggregate, the distribution of its fragments has been approximated by binary, ternary and normal distribution functions [26,38]). Binary and ternary unctions are simplified formulations, while the normal distribution is considered to be a more realistic description. However, these three distribution functions do not differ significantly according to our previous study on the role of breakage in the formation of particle size distribution [28]. Thus, simple binary breakage is employed here as the fragment distribution function. Binary breakage means the breakup of an aggregate into two equal fragments, which has the distribution form

$$\gamma(m,'' m) = \begin{cases} 2 & (m = m''/2), \\ 0 & (m \neq m''/2). \end{cases} \tag{10}$$

2.5. Modelling and simulation conditions

Numerical simulations were performed for PSD dynamics in marine waters, which is an open particle system with consistent particle fluxes into and out of the mixed water column. Three scenarios were investigated, with different combinations of collision models and simulation conditions. For scenario A, the rectilinear collision model and the assumptions described above for dimensional analysis (DA assumptions) were used; for scenario B, the curvilinear collision model was used without the DA assumptions, i.e., collisions occur between particles of all sizes, and particles of all sizes can be removed from the system by sedimentation; for scenario C, the curvilinear model was also used without the DA assumptions, and the particle breakup process was included. Fractal scaling properties were incorporated into the modelling simulations.

The density of the primary particles was $1.2\,g\,cm^{-3}$. The initial particle concentration was $Q_0 = 5.0 \times 10^{-5}\,g\,cm^{-3}$ in a mono-dispersion. The size of the primary particles was usually 0.1 μm, while an input at 0.01 μm as well as a simultaneous input of three primary particles at 0.1, 1.0 and 10.0 μm were also tested. The normal conditions had a shear intensity of $G = 0.5\,s^{-1}$ and a particle input rate of $q_{in} = 5.0 \times 10^{-10}\,g\,cm^{-3}\,s^{-1}$. Both parameters were varied, and the responses of the PSD in the system were examined. It is generally agreed that an increase in the particle collision efficiency would result in faster coagulation and the formation of particle aggregates with a lower fractal dimension [21,29,34,40]. Thus, three combinations of the fractal dimension and collision efficiency were used in the present simulation study: (1) $D = 3.0$ and $\alpha = 0.1$, (2) $D = 2.5$ and $\alpha = 0.3$ and (3) $D = 2.0$ and $\alpha = 0.5$. In addition, a change in the collision efficiency from $\alpha = 0.01$ to 1.0 was tested. The whole size range with 48 contiguous size sections was from 0.1 μm to approximately 1 cm for non-fractal particles, and this extended further for fractal particle aggregates. Other coefficients and constants included the depth of the mixing water layer $H = 5.0\,m$, temperature $T = 298\,K$, liquid density $\rho_l = 1.0\,g\,cm^{-3}$, viscosity $\mu = 8.9 \times 10^{-3}\,g\,s^{-1}\,cm^{-1}$, Boltzmann's constant $k = 1.38 \times 10^{-16}\,g\,cm^2\,s^{-2}\,K^{-1}$ and the gravitational constant $g = 981\,cm\,s^{-2}$. The program was written in the *Compaq Fortran* (formerly DIGITAL Fortran) programming language, which includes *Fortrans 95* and *90*, and runs on a PC under *Windows 98*. There were occasional negative values for particle concentrations in the numerical simulations. However, based on the sensitivity test for the computation time-step, this problem disappeared when the time step was shortened to 1 s.

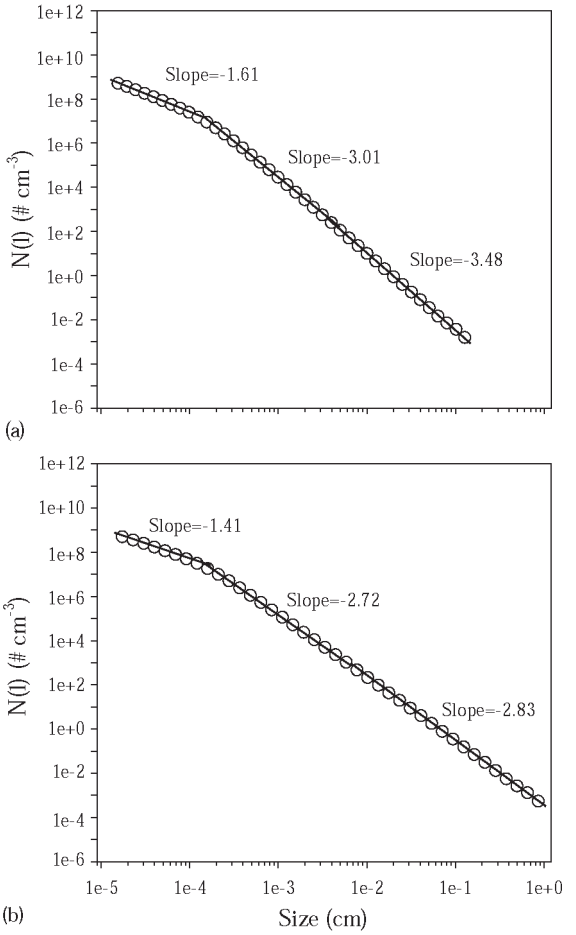

Fig. 1. Simulated cumulative particle size distributions based on the rectilinear model and the DA assumptions for marine particles with fractal dimensions of (a) $D = 3.0$, and (b) $D = 2.5$.

3. Results and discussion

3.1. Simulations based on the rectilinear model and DA assumptions

A dynamic steady state in particle size distribution can be reached after a period of simulation, accounting for particle influx, coagulation and sedimentation, and regardless of the initial conditions. The simulations based on the rectilinear collision model and the assumptions used for dimensional analysis give three linear regions with different slopes in a typical cumulative particle size distribution after log–log transformation (Fig. 1a). As suggested by previous dimensional analysis [1,11], different collision mechanisms apparently dominate in different size ranges, resulting in different PSD slopes. For small particles ranging from 0.1 to 2 μm, Brownian motion is believed to be the dominant mechanism for particle collisions, which produces a size distribution with a slope of −1.61. In the size range approximately from 2 to 60 μm, where fluid shear is considered to dominate, the PSD slope is −3.01. For particles larger than 60 μm, differential sedimentation becomes dominant, which leads to a PSD with a steeper slope of −3.48.

When fractal scaling is incorporated for particle characterization, three linear regions with different slopes can also be identified in the size distribution (Fig. 1b). The major change with the inclusion of fractal mathematics is that the PSD lines become flatter, i.e., the slope decreases with the value of the fractal dimension. For example, as D decreases from 3.0 to 2.5, the slope changes from −1.61 to −1.41 for small particles in the size range dominated by Brownian motion, from −3.01 to −2.72 for particles in the range of shear collisions, and from −3.48 to −2.83 for the size range of differential sedimentation.

The values of the simulated PSD slopes compare well with those previously predicted by dimensional analysis based on the same rectilinear model and assumptions [1,13] (Table 3). In the size ranges dominated by fluid shear and differential sedimentation, there is an excellent agreement of the slope between the dimensional analysis values and the simulation results. For small particles dominated by Brownian motion, the simulated slopes are slightly steeper than those determined by dimensional analysis (Table 3). According to additional simulations, the likely cause for the steeper slopes is that the primary particles may not be small enough for the narrow range from 0.1 to 2 μm. If the size range is expanded to a much smaller size of the primary particles, e.g., 0.01 μm, then the simulated slopes become −1.55 for particles with $D = 3.0$, −1.30 for $D = 2.5$, and −1.05 for $D = 2.0$. These revised slopes are closer to the dimensional analysis values (Table 3), while the slopes in the size ranges of shear collisions and differential sedimentation are hardly affected by a change in the size of primary particles.

With the rectilinear collision model employed, DA assumptions, particularly the one assuming that collisions occur only between like-sized particles, have to be used collectively for the PSD simulations. If the assumptions were not applied, collisions would take place between particles of all sizes rather than just between those of similar sizes. The steady-state PSD simulated is no longer a smooth line in the full size range (Fig. 2), and only a short linear region where Brownian motion dominates can be found. This modelling result does not appear to be realistic, and is completely different from the observations of PSD from many field and laboratory studies (Table 1). The PSD curves simulated in Fig. 2 imply that both the rectilinear model and the DA assumptions need to be applied together for a reasonable simulation of the steady-state PSD in the ocean.

3.2. Simulations based on the curvilinear model without the DA assumptions

It has been well accepted that the curvilinear model is more applicable than the rectilinear model to describe the collision kinetics of the particles in which permeability is not considered. In the following simulations, the curvilinear model is used for particle dynamics

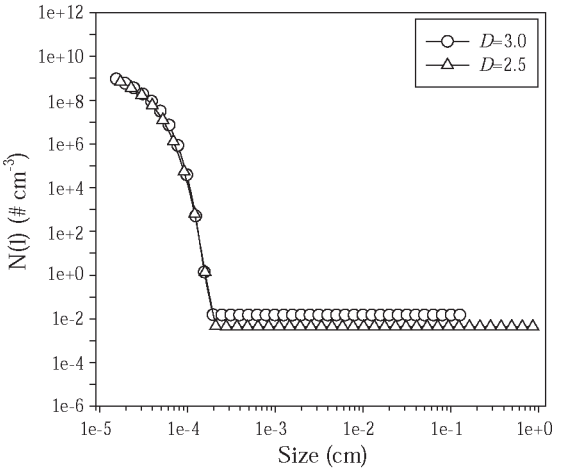

Fig. 2. Simulated cumulative particle size distributions based on the rectilinear model without the DA assumptions for particles with fractal dimensions of 3.0 and 2.5.

Table 3
PSD slopes and particle concentrations predicted by dimensional analysis (DA) and numerical simulations

Dominant collision mechanism assumed Approximate size range	Brownian motion <2 μm	Fluid shear 2∼60 μm	Differential sedimentation >60 μm	Particle concentration ($\times 10^4$ g cm^{-3})
$D = 3.0$, DA prediction	−1.50	−3.00	−3.50	—
Simulation				
A	−1.61 (−1.55)	−3.01 (−3.03)	−3.48 (−3.47)	2.16
B	−1.60	−2.87	—	2.35
C	−1.58	−2.70	—	2.85
$D = 2.5$, DA prediction	−1.25	−2.75	−3.00	—
Simulation:				
A	−1.41 (−1.30)	−2.72 (−2.69)	−2.83 (−2.79)	0.61
B	−1.38	−2.55	−2.75	0.81
C	−1.37	−2.53	−2.73	1.06
$D = 2.0$, DA prediction	−1.00	−2.50	−2.50	—
Simulation:				
A	−1.18 (−1.05)	−2.42 (−2.54)	−2.50 (−2.52)	0.29
B	−1.17	−2.38	−2.32	0.30
C	−1.17	−2.39	−2.13	1.25

Note: (A) Rectilinear model + DA assumptions, data in ( ) are for the input of the primary particles at 0.01 μm; (B) Curvilinear model (without the DA assumptions); (C) Curvilinear model + breakage function (without the DA assumptions).

without the assumptions made in the dimensional analysis approach. As in the rectilinear results, there are different linear regions with different slopes that can be identified in the cumulative particle size distributions. The three collision mechanisms apparently operate in different size ranges, while the fractal dimension also plays an important role in determining the PSD slope (Fig. 3). Compared with the rectilinear cases, a significant alteration in the distribution curve can be found in the size range of larger particles. For particles with a higher fractal dimension approaching 3.0, the PSD becomes much steeper, with a slope of about −20 (Fig. 3a). As the fractal dimension value decreases, the PSD slope in this portion becomes flatter (Fig. 3b). With a fractal dimension of 2.0, the slope for the large particles changes to −2.32 (Fig. 3c).

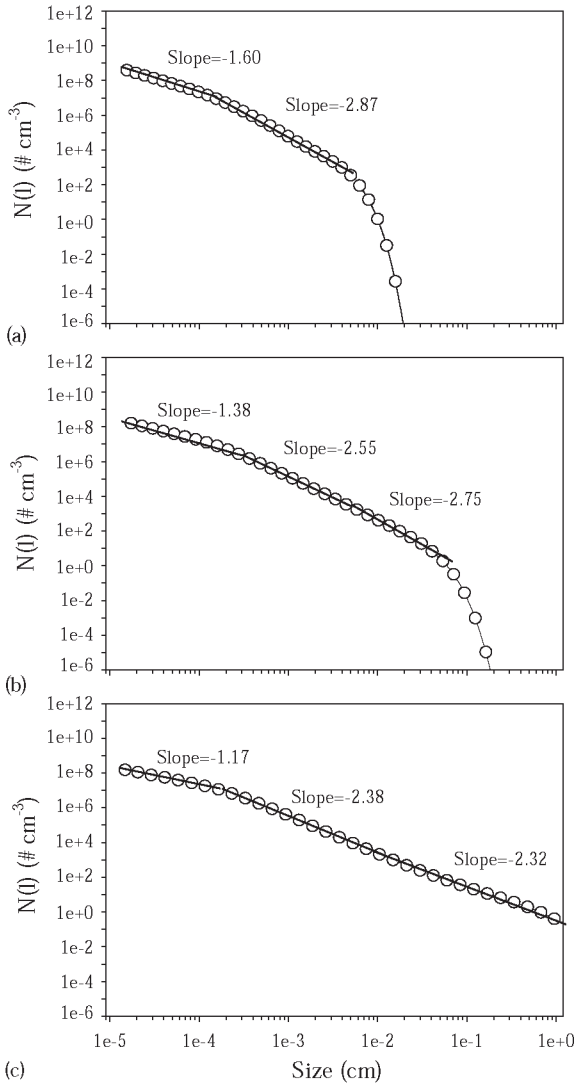

Fig. 3. Simulated cumulative particle size distributions based on the curvilinear model without the DA assumptions for marine particles with fractal dimensions of (a) $D = 3.0$, (b) $D = 2.5$, and (c) $D = 2.0$.

The simulation results obtained with the more accurate curvilinear model without the unrealistic DA assumptions validate the important generality for the particle size distribution in marine waters. The environmental conditions, such as the intensity of fluid shear, the rate and size of particle input into the system, and the nature of the particles, do not appear to affect the general shape of the PSD curve. For example, for particles with $D = 2.5$, as the shear rate increases from 0.5 to $5\,s^{-1}$, the position of the PSD curve is slightly lower. However, the size distribution remains the same shape, with virtually the same slopes, for the three linear regions (Fig. 4a). As the particles become less sticky, with α changing from 0.3 to 0.03, the particle concentration increases and the position of the PSD curve moves up considerably. However, the shape and slopes of the distribution are hardly affected (Fig. 4a). With an increase in the rate of particle influx from 5×10^{-10} to $5 \times 10^{-8}\,g\,cm^{-3}\,s^{-1}$, particle population increases for all sizes, but the PSD slopes remain almost unchanged (Fig. 4b). If the same input of $5 \times 10^{-10}\,g\,cm^{-3}\,s^{-1}$ occurs equally in the three classes of primary particles at 0.1, 1 and 10 μm, the PSD result is almost identical to the situation when there is only an input of primary particles of 0.1 μm, except for a slight decrease in the slope in the size range of small particles.

It is also worth noting that the PSD slopes predicted by dimensional analysis with the rectilinear model compare fairly well with those simulated using the curvilinear model without additional assumptions, particularly in the size range of small particles (Table 3). The rectilinear model is known as the simplest description of collision kinetics that over-predicts particle collisions [20,21,30,34]. As the particle system becomes more heterogeneous, coagulation could be largely accelerated with the rectilinear model [20,28]. On the other hand, however, the DA assumption about collisions occurring only between particles of similar sizes leads to an under-prediction of the coagulation rate. In actuality, there are abundant particles over a wide spectrum of sizes. Collisions occur between particles of all sizes, and all of the three collision mechanisms are involved. In the scheme for the sectional method, for example, a primary particle has a chance of becoming attached to any of the larger particles and arriving in a larger size section, rather than coagulating with other primary particles only. Therefore, the opposite effects of the DA assumptions, which underestimate the collision frequencies, and the rectilinear model, which overestimates the collision frequencies, may largely offset each other and result in a rather reasonable calculation of the coagulation rates.

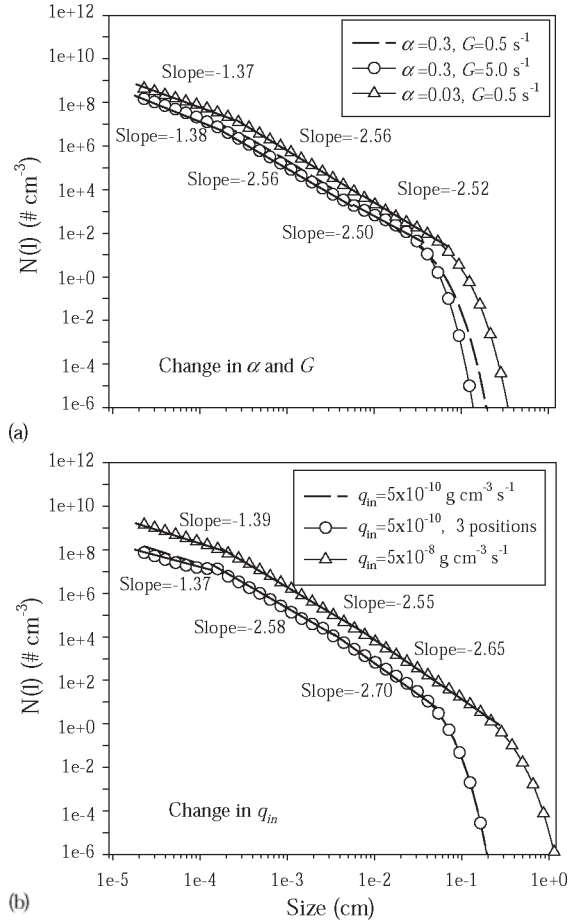

Fig. 4. Effects of particle properties and process variables on the particle size distribution when: (a) the collision efficiency decreases from 0.3 to 0.03, and the shear intensity increases from 0.5 to 5 s^{-1}, and (b) the particle input pattern changes from a single class of primary particles of 0.1 μm to three classes of primary particles of 0.1, 1, and 10 μm, and the influx of primary particles increases from 5×10^{-10} to 5×10^{-8} g cm^{-3} s^{-1}. The simulations are based on the curvilinear model without the DA assumptions for particles of $D=2.5$.

Using the curvilinear model of Han and Lawler [20], the magnitude of the curvilinear reductions given in Eq. (7) increases dramatically as the difference between the sizes of colliding particles increases. For example, the reduction factor for shear coagulation could change from 0.5 to 10^{-4} or below as the size ratio of two particles decreases from 1 to 0.1. Thus, the curvilinear model actually gives much more importance to collisions between like-sized particles in the coagulation process, although interactions between particles of all sizes are taken into account. The mathematical treatment of the curvilinear model actually created a situation that is to a certain extent similar to the DA assumption of collisions taking place only between similarly sized particles. As a result, the simulations from the rectilinear scenario with the DA assumptions and the curvilinear scenario without the DA assumptions for the PSD slopes do not differ extensively, although the positions of the PSD and related particle populations from different simulation scenarios are different from one another. In general, as far as the shape of the PSD curve is concerned, the analytical solutions from previous dimensional analysis still offer valuable approximations for PSD slopes in marine waters.

3.3. Effects of the breakage process

The effect of aggregate breakup on the steady-state PSD increases with the degree of shear intensity and decreases with the magnitude of the fractal dimension, especially in the size range of large particles. For particles of $D=2.5$, the PSD, with the inclusion of the breakage function at $G=0.5\,s^{-1}$, is nearly the same as that without accounting for the breakup process (Fig. 5a). As the shear rate increases to 5 s^{-1}, the size distribution of small particles for which Brownian motion and shear collisions are dominant is still not seriously affected by particle breakage. The size distribution of large particles, however, is altered. There are fewer particles larger than 600 μm left in the PSD, apparently due to aggregate breakage, and the distribution curve becomes steeper as a result. The fragments of the broken aggregates accumulate in the intermediate size range from 60 to 600 μm, in which the PSD becomes flatter and the slope changes to −2.50 from the original −2.75 without breakage being considered.

For more fractal particles with $D=2.0$, particle breakage by fluid shear also shows no significant effect on the size distribution of small particles (Table 3). However, the PSD of large particles is further modified. With an increase in the shear intensity from 0.5 to 5 s^{-1}, particles larger than 2000 μm decrease in concentration and their distribution changes from an approximately straight line to a descending curve. There is a further accumulation of particles in the intermediate size range from 100 to 2000 μm. Large fractal aggregates are broken up by a higher degree of fluid turbulence. More fragments fall into the intermediate size range, resulting in a rather flat slope of −1.63 (Fig. 5b).

Unlike coagulation, which transforms small particles into larger aggregates, breakage turns large particles into smaller ones. Since the settling velocity decreases with the size of the particle, breakage keeps the particulate material in suspension in the water column for a longer time. Larger and more fractal particle aggregates are more vulnerable to breakup by the shear of fluid turbulence than smaller and non-fractal particles [27,28]. Breakage impedes the continuous formation of larger particles and prevents the trend of particle size

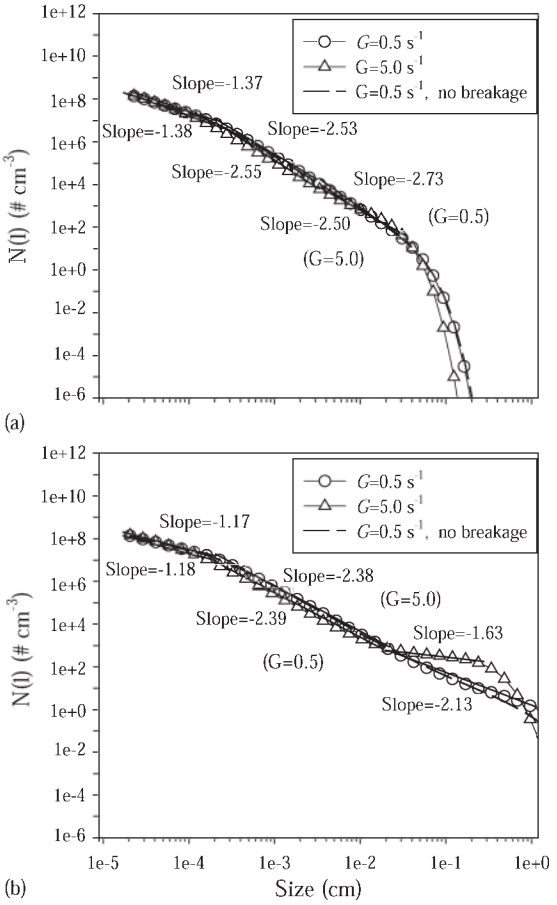

Fig. 5. Effects of particle breakage on the size distributions of particles with fractal dimensions of (a) $D = 2.5$ and (b) $D = 2.0$ at shear intensities of 0.5 and $5\,s^{-1}$, in comparison to no breakage cases. The simulations are based on the curvilinear model without the DA assumptions.

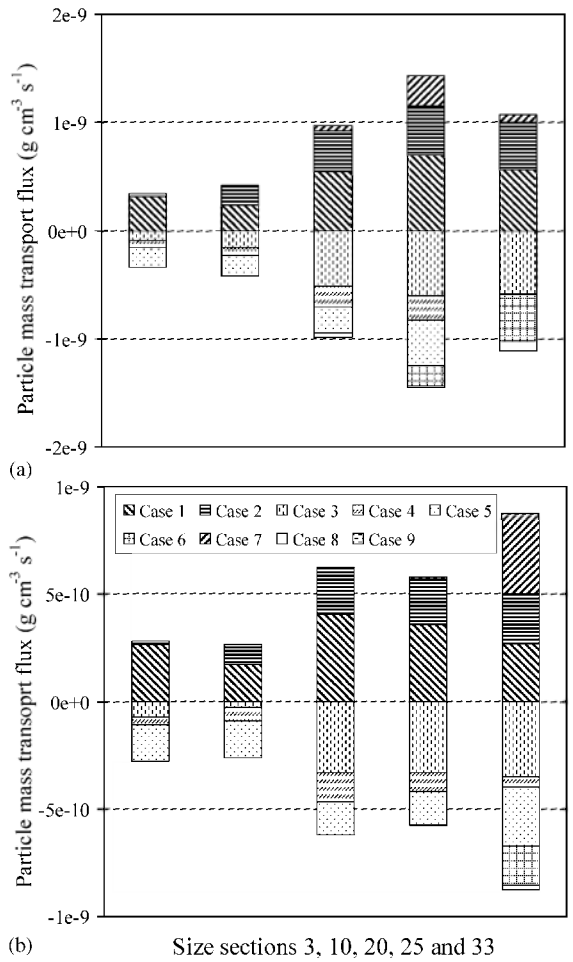

Fig. 6. Particle mass transport fluxes into and out of a size section brought about by the nine transport cases indicated in Eq. (2) and Table 2 for the selected size sections under the simulation conditions of (a) $D = 2.5$ and $G = 5.0\,s^{-1}$ and (b) $D = 2.0$ and $G = 0.5\,s^{-1}$. The simulations are based on the curvilinear model without the DA assumptions for the size distributions in the steady state with a constant particle influx of $5 \times 10^{-10}\,g\,cm^{-3}\,s^{-1}$.

growth. As a result, particles accumulate within a certain size range. This finding agrees well with the simulation results of Burd and Jackson [14]. The degree of particle accumulation depends on the balance between the two processes of coagulation and breakage. In general, however, given the low intensity of fluid shear in the ocean, the present simulation does not suggest an important role for breakage in the formation of marine PSD. Only at a higher degree of fluid turbulence could the impact of breakage become important to the size distribution of large particles that usually are highly fractal in nature [5,18,19].

As depicted by the governing equation (2), all particle transport and transformation processes, including coagulation, breakup, sedimentation and influx, influence the PSD dynamics. For additional examination of the numerical simulation, the particle mass fluxes brought about by the nine individual transport cases given in Table 2 are plotted in Fig. 6 for a number of selected size sections. These transport flux terms that cause either gain or loss of particle mass take place all the time and contribute to various extents to the mass concentration of particles in a section. However, the sum of mass gain terms is always well balanced by the sum of mass loss terms for any PSD section in its steady state (Fig. 6). Thus, a stable PSD can be maintained in the system with constant concentrations in all size sections.

3.4. Implications of PSD dynamics

Many field observations have shown a power-law size distribution of particles in the ocean (Table 1). The slope appears to vary only within a relatively narrow range

mainly from −1.5 to −4.0, despite the differences in particle properties and the water environment. The present simulations demonstrated that the PSD slope is mainly a function of the size range and fractal dimension of the particles. The shape of the PSD is generally not regulated by the nature of the particles, the rate and pattern of particle input, or other physical and chemical factors. With the demonstrated generality of PSD for marine particles, and particularly for particles which are not much larger than 100 μm, the degree of variation in the slope observed in the field becomes an issue that has not been addressed. It is argued that non-steady-state conditions in natural waters could be the main reason for the deviation in PSD slopes.

Due to frequent changes in the natural conditions, such as rain, wind, current and fluid shear intensity, as well as changes in the input rate and the characteristics of the particles, the size distribution in the ocean may not stay in a consistent steady state. The PSD may frequently be transformed from one steady state to another by changes in the environmental variables. As the PSD moves in position, its slope also varies from time to time. For example, as the particle influx rate increases from 5×10^{-10} to $5\times10^{-8}\,\mathrm{g\,cm^{-3}\,s^{-1}}$, the original PSD steady state will not be maintained, and the particle system will approach a new steady state. After 40,000 s of simulation, a new steady state is reached with a higher particle concentration. Although the new PSD slope in a different size range is almost unchanged, its position is higher than the previous one (Fig. 7a). During the transition from the previous steady state to the new steady state, the concentration of small particles initially increases with the higher rate of particle input. The concentration then increases gradually through the size distribution from the size sections of small particles to the sections of larger particles until the new steady state is reached. During this transition phase, the PSD slope increases in the early phase and then decreases, instead of remaining at the same value.

In addition, the nature of the particles, especially phytoplankton and other biological particles, often changes with time. For example, during an algal bloom, the cells could become stickier toward the end of the bloom [8,47,48]. Such a change in the property of the particles would result in a higher collision efficiency and thus faster aggregation. According to the simulation, as α increases from 0.01 to 1.0, the mass concentration of particles in the system decreases considerably when the new steady state is reached. The position of the size distribution changes, although the slopes in different size ranges are almost unaffected (Fig. 7b). A higher collision efficiency enhances particle flocculation, which forces small particles into larger size sections that can readily be removed from the water by sedimentation. The amount of small particles decreases continuously, while the amount of large particles first increases with

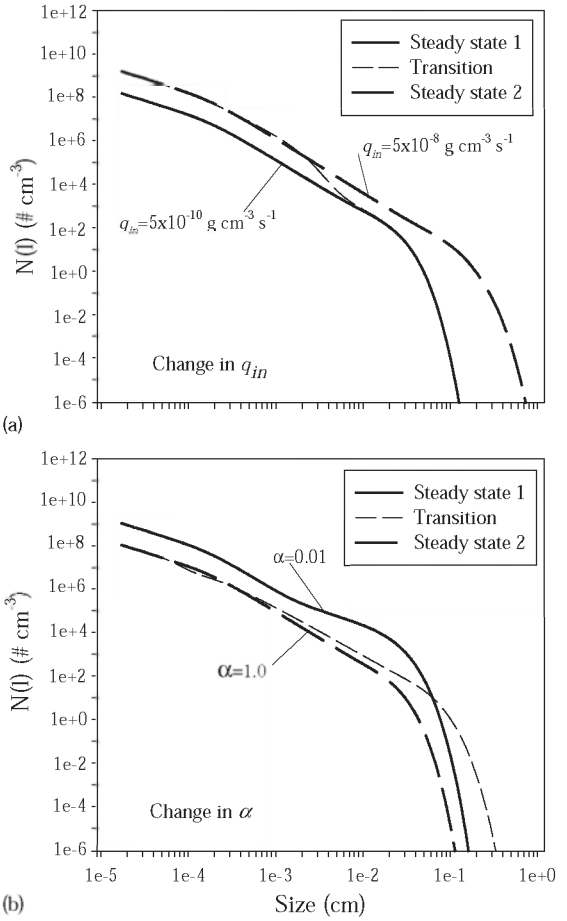

Fig. 7. Transitions of particle size distributions between different steady states as (a) the particle influx rate increases from 5×10^{-10} to $5\times10^{-8}\,\mathrm{g\,cm^{-3}\,s^{-1}}$ and (b) the collision efficiency increases from 0.01 to 1.0. The simulations are based on the curvilinear model without the DA assumptions for particles of $D=2.5$. Shear breakage at $G=0.5\,\mathrm{s^{-1}}$ is included.

coagulation and then decreases through sedimentation. Therefore, the transition of the PSD from one steady state to another in natural waters may often result in shifting of the slope within a certain range, as observed in the field (Table 1).

The slope is the single most important parameter for characterizing the shape of the particle size distribution. With the generality in the steady-state PSD demonstrated by the present simulation, the variation in the actual slope provides a useful insight into particle dynamics in marine waters. A higher value of the slope (a steeper slope) may be related to the rapid input of new particles of specific sizes, such as a phytoplankton bloom, additional surface runoff, or wastewater discharge. A lower value of the slope (a flatter slope) may indicate the importance of particle coagulation in the system [5,9,49]. In previous field studies in the spring in

eastern Pacific coastal waters, one in East Sound, WA, and the other in Monterey Bay, CA, USA, the PSD slopes observed in the two different sites were not consistent with each other. A steeper size distribution with an average slope of around −2.0 was determined for the samples in East Sound, where a phytoplankton (*Phaeocystis pouchetii*) bloom was found in its early stages [5]. The later development of the bloom was unclear owing to the limited period of the field survey. In Monterey Bay, the measurement showed a flatter PSD with an average slope of around −1.5. A relatively low concentration of small particles was observed, together with a large number of diatom flocs, including marine snow-sized flocs [5]. In this water, coagulation could be an important means of transforming small particles into larger aggregates following a likely spring bloom. The change in the PSD slope driven by coagulation was further demonstrated by a diatom bloom generated in a laboratory mesocosm further [2,30]. After 7 days of inoculation, flocculation of the diatom cells in the tank became increasingly important, forcing the slope to change from −1.77 to −1.20. These field and laboratory observations are in good agreement with the findings of the present simulation for PSD-related particle population dynamics.

4. Conclusions

Particle influx and interactions are essential in determining the general shape of the particle size distribution in the ocean. Based on the fractal-curvilinear coagulation model, the particle size distribution dynamics in marine waters can be simulated by accounting for particle input, coagulation, sedimentation and breakage. A steady-state PSD can be established after a period of simulation regardless of the initial conditions. There are three linear regions in the cumulative PSD after log–log transformation with different slopes corresponding to the collision mechanisms of Brownian motion, fluid shear and differential sedimentation. The PSD slope varies from −3.5 to −1.2 as a function of the size range and the fractal dimension of the particles concerned. The simulation results agree well with many field observations in the ocean in terms of the generality in the shape of the steady-state PSD. The environmental conditions, such as the intensity of fluid shear, the rate and size of particle influx into the water, and the particle properties, such as the type and collision efficiency of the particles, do not seriously affect the PSD slope, although they may change the PSD position and related particle concentrations. Breakage has virtually no effect on the size distribution of small particles, while a strong shear may cause a considerable change in the PSD for larger and fractal particles. The simplified dimensional analysis approach developed by Hunt [1] and Jiang and Logan [13] still offers helpful approximations for the PSD slopes, although the previous solutions are not always consistent with the simulation results. A certain degree of variation in the PSD slope that has been observed in the field also can be mathematically demonstrated. It is suggested that, owing to the complex nature of particles and water environments, the size distribution could be altered by inconsistent particle input or non-steady-state coagulation. The PSD slope would vary with time during the transition stage of the size distribution. An increase in the slope value may be caused by a greater input of particles that have yet coagulated, while a decrease in the slope may suggest a well-flocculated particle system. Therefore, the PSD modelling has important implications for better descriptions of the interactions and transport of particulate matter, including biomass and organic pollutants, in the ocean.

Acknowledgements

This research was supported by grants HKU7327/98E and HKU2/98C from the Research Grants Council of the Hong Kong SAR Government, China.

References

[1] Hunt JR. Prediction of oceanic particle size distributions from coagulation and sedimentation mechanisms. Adv Chem Ser 1980;189:243–57.
[2] Jackson GA, Logan BE, Alldredge AL, Dam HG. Combining particle size spectra from a mesocosm experiment measured using photographic and aperture impedance (Coulter and Elzone) techniques. Deep-Sea Res 1995;42:139–57.
[3] Jonasz M, Fournier G. Approximation of the size distribution of marine particles by a sum of log-normal functions. Limnol Oceanogr 1996;41:744–54.
[4] Lambert CE, Jehanno C, Silverberg N, Brun-Cottan JC, Chesselet R. Log-normal distributions of suspended particles in the open ocean. J Mar Res 1981;39:77–89.
[5] Li XY, Passow U, Logan BE. Fractal dimension of small (15–200 μm) particles in Eastern Pacific coastal waters. Deep-Sea Res 1998;45:115–31.
[6] McCave IN. Size spectra and aggregation of suspended particles in the deep ocean. Deep-Sea Res 1984;31:329–52.
[7] Sheldon RW, Prakash A, Sutcliff WH. The size distribution of particles in the ocean. Limnol Oceanogr 1972; 17:327–40.
[8] Alldredge AL, Passow U, Logan BE. The abundance and significance of a class of large, transparent organic particles in the ocean. Deep-Sea Res 1993;40:1131–40.
[9] Gardner DG, Walsh ID. Distribution of macroaggregates and fine-grained particles across a continental margin and their potential role in fluxes. Deep-Sea Res 1990;37: 401–11.

[10] Hill PS. Reconciling aggregation theory with observed vertical fluxes following phytoplankton blooms. J. Geophys Res 1992;97(C2):2295–308.
[11] Hunt JR. Self-similar particle-size distributions during coagulation: theory and experimental verification. J Fluid Mech 1982;122:169–85.
[12] Jackson GA, Lochmann SE. Modeling coagulation of algae in marine ecosystems. In: Buffle J, van Leeuwen HP, editors. Environmental particles 2. Boca Raton, FL, USA: Lewis; 1993. p. 387–414.
[13] Jiang Q, Logan BE. Fractal dimensions of aggregates determined from steady-state size distributions. Environ Sci Technol 1991;25:2031–8.
[14] Burd AB, Jackson GA. Modeling steady-state particle size spectra. Environ Sci Technol 2002;36:323–7.
[15] Jackson GA. A model of the formation of marine algal flocs by physical coagulation processes. Deep-Sea Res 1990;37:1197–211.
[16] Jackson GA. Using fractal scaling and two-dimensional particles size spectra to calculate coagulation rates for heterogeneous systems. J Colloid Interface Sci 1998;202: 20–9.
[17] Li XY, Zhang JJ. Numerical simulation and experimental verification of particle coagulation dynamics for a pulsed input. J Colloid Interface Sci 2003;262:149–61.
[18] Kilps JR, Logan BE, Alldredge AL. Fractal dimensions of marine snow aggregates determined from image analysis of in situ photographs. Deep-Sea Res 1994;41:1159–69.
[19] Logan BE, Wilkinson DB. Fractal geometry of marine snow and other biological aggregates. Limnol Oceanogr 1990;35:130–6.
[20] Han MY, Lawler DF. The (relative) insignificance of G in flocculation. J AWWA 1992;84(10):79–91.
[21] Li XY, Logan BE. Collision frequencies between fractal aggregates and small particles in turbulently sheared fluid. Environ Sci Technol 1997;31:1237–42.
[22] Veerapaneni S, Wiesner MR. Hydrodynamics of fractal aggregates with radially varying permeability. J Colloid Interface Sci 1996;177:45–57.
[23] Gelbard FY, Tambour Y, Seinfeld JH. Sectional representations for simulating aerosol dynamics. J Colloid Interface Sci 1980;76:541–56.
[24] Hounslow MJ, Ryall RL, Marshall VR. A discretized population balance for nucleation, growth and aggregation. AIChE J 1988;34:1821–32.
[25] Thomas DN, Judd SJ, Fawcett N. Flocculation modelling: a review. Water Res 1999;33:1579–92.
[26] Flesch JC, Spicer PT, Pratsinis SE. Laminar and turbulent shear-induced flocculation of fractal aggregates. AIChE J 1999;45:1114–24.
[27] Spicer PT, Pratsinis SE. Coagulation and fragmentation: universal steady-state particle-size distribution. AIChE J 1996;42:1612–20.
[28] Zhang JJ, Li XY. Modeling particle size distribution dynamics in a flocculation system. AIChE J 2003; 49(7):1870–82.
[29] Meakin P. Fractal aggregates. Adv Colloid Interface Sci 1988;28:249–331.
[30] Li XY, Logan BE. Size distribution and fractal properties of particles during a simulated phytoplankton bloom in mesocosm. Deep-Sea Res 1995;42:125–38.
[31] Johnson CP, Li XY, Logan BE. Settling velocities of fractal aggregates. Environ Sci Technol 1996;30:1911–8.
[32] Li XY, Yuan Y. Collision frequencies of microbial aggregates with small particles by differential sedimentation. Environ Sci Technol 2002;36:387–93.
[33] Adler PM. Heterocoagulation in shear flow. J Colloid Interface Sci 1981;83:106–15.
[34] O'Melia CR, Tiller CL. Physicochemical aggregation and deposition in aquatic environments. In: Buffle J, van Leeuwen HP, editors. Environmental particles 2. Boca Raton, FL, USA: Lewis; 1993. p. 252–86.
[35] Pandya JD, Spielman. Floc breakage in agitated suspensions: theory and data processing strategy. J Colloid Interface Sci 1982;90:517–26.
[36] Potanin AA. On the mechanism of aggregation in the shear flow of suspension. J Colloid Interface Sci 1991;145:140–57.
[37] Yeung AKC, Pelton R. Micromechanics: a new approach to studying the strength and break-up of flocs. J Colloid Interface Sci 1996;184:579–85.
[38] Chen W, Fisher RR, Berg JC. Simulation of particle size distribution in an aggregation-breakup process. Chem Eng Sci 1990;45:3003–6.
[39] Serra T, Casamitjana X. Effect of the shear and volume fraction on the aggregation and breakup of particles. AIChE J 1998;44:1724–30.
[40] Jiang Q, Logan BE. Fractal dimensions of aggregates from shear devices. J AWWA 1996;88(2):100–13.
[41] McCave IN. Vertical flux of particles in ocean. Deep-Sea Res 1975;22:491–502.
[42] Lerman A, Carder KL, Betzer PR. Elimination of fine suspensoids in oceanic water column. Earth Planet Sci Lett 1977;37:61–70.
[43] Harris JE. Characterization of suspended matter in the Gulf of Mexico-II: particle size analysis of suspended matter from deep water. Deep-Sea Res 1977;24:1055–61.
[44] Bishop JKB. The chemistry, biology, and vertical flux of particulate matter from the upper 400 m of the Cape Basin in the southeast Atlantic Ocean. Deep-Sea Res 1978; 25:1121–61.
[45] Baker ET, Feely RA, Takahashi K. Chemical composition, size distribution and particle morphology of suspended particulate matter at DOMES site A, B, and C: relationships with local sediment composition. In: Bischoff JL, Piper DZ, editors. Marine geology and oceanography of the Pacific Manganese Nodule Province. New York: Plenum Press; 1979. p. 163–201.
[46] Bishop JKB, Collier RW, Ketten DR, Edmond JM. The chemistry, biology, and vertical flux of particulate matter from the upper 1500 m of the Panama Basin. Deep-Sea Res 1980;27:615–40.
[47] Kiørboe T, Olesen M. Phytoplankton aggregation formation-observations of patterns and mechanisms of cell sticking and the significance of exopolymeric material. J Plankton Res 1993;15:993–1018.
[48] Engel A. The role of transparent exopolymer particles (TEP) in the increase in apparent particle stickiness (α) during the decline of a diatom bloom. J Plankton Res 2000;22:485–97.
[49] Jackson GA. Comparing observed changes in particle size spectra with those predicted using coagulation theory. Deep-Sea Res 1995;42:159–84.